International Journal of Greenhouse Gas Control 32 (2015) 197–212

Contents lists available at ScienceDirect

International Journal of Greenhouse Gas Control

journal homepage: www.elsevier.com/locate/ijggc

Modeling the CO_2-based enhanced geothermal system (EGS) paired with integrated gasification combined cycle (IGCC) for symbiotic integration of carbon dioxide sequestration with geothermal heat utilization

Arun Ram Mohan[a], Uday Turaga[b], Viswanathan Subbaraman[c], Vishakha Shembekar[d], Derek Elsworth[a], Sarma V. Pisupati[a,*]

[a] John and Willie Leone Department of Energy and Mineral Engineering and The EMS Energy Institute, The Pennsylvania State University, University Park, PA 16802, USA
[b] ADI Analytics LLC, 14511 Old Katy Rd, Suite 374, Houston, TX, USA
[c] SSTD Inc, Houston, TX, USA
[d] Omkar Scientific Solutions LLC, 3133 Buffalo Speedway Apt 1309, Houston, TX, USA

ARTICLE INFO

Article history:
Received 25 January 2014
Received in revised form 7 October 2014
Accepted 16 October 2014

Keywords:
CO_2 sequestration
Coal combustion
IGCC
Enhanced geothermal systems

ABSTRACT

The global warming potential of carbon dioxide (CO_2) emphasizes more the sequestration of CO_2 otherwise emitted from coal-fired power plants in the future. This study is focused on pairing a coal-fired integrated gasification combined cycle (IGCC) plant with enhanced geothermal system (EGS) for simultaneous sequestration of CO_2 and extraction of geothermal heat energy for subsequent electricity generation by an organic Rankine cycle (ORC) in enhanced geothermal systems (EGS). By assuming the reservoir characteristics for two different geothermal source temperatures 200 °C and 300 °C, heat transfer calculations show that larger reservoir volume (>1 km^3) is necessary for the sustained extraction of geothermal heat energy over a period of 25 years. The temperature and pressure profiles of CO_2 in the injection well and the production well, the corresponding power output from the ORC for five different working fluids, are simulated by ASPEN Plus Version 7.3. The reservoir conditions and the type of working fluid selected determine the power output in the ORC. The temperature and the pressure of the CO_2 at the outlet of the production well are greater than that at the injection well due to the heating of CO_2 in the reservoir during the extraction of geothermal heat energy. Therefore, a combination of a high pressure turbine and an organic Rankine cycle is beneficial for the conversion of geothermal energy from CO_2 into electricity before its recirculation into the injection well. Among the secondary working fluids used in the modeling of the ORC, the time-averaged net EGS power is highest for isobutane and lowest for isopentane over a period of 25 years. When isobutane is used as a secondary working fluid, the time-averaged power output over a period of 25 years for two geothermal reservoirs at an initial geothermal source temperature of 300 °C and 200 °C are 46 MW_e and 21 MW_e, respectively. When neopentane is used as a secondary working fluid, the time-averaged power output for a period of 25 years is 37 MW_e for an initial geothermal source temperature of 300 °C and 17 MW_e for an initial geothermal source temperature of 200 °C. Pairing IGCC with EGS can considerably recover some of the energy lost during the sequestration of CO_2 (50 MW_e) from a 629 MW_e IGCC plant.

1. Introduction

The total amount of the geothermal energy resource base in the United States is approximately 14×10^6 EJ (exajoules) at depths between 3 km and 10 km (The Future of Geotherrmal Energy, 2006). At a depth of 6.5 km, the amount of geothermal energy is estimated to be 600,000 EJ and 10,000 EJ for a geothermal source temperature of 200 °C and 300 °C, respectively (The Future of Geotherrmal Energy, 2006). The total amount of electricity generated in the United States in 2011 was 14×10^{18} J (US Energy Information, 2012). Electricity generation from geothermal energy in the United States in 2011 was 60×10^{15} J (US Energy Information, 2011). This

* Corresponding author. Tel.: +1 814 865 0874; fax: +1 814 865 3248.
E-mail addresses: spisupati@psu.edu, sxp17@psu.edu (S.V. Pisupati).

http://dx.doi.org/10.1016/j.ijggc.2014.10.016
1750-5836/

Nomenclature

L	length of the fracture (m)
W	width of the fracture (m)
H	height of the fracture (m)
S	fracture spacing (m)
α	permeability of the reservoir (m^2)
ε	porosity of the reservoir
V	total rock volume (m^3)
V_V	void volume
V_F	volume of each fracture
L_F	length of the fracture
A_c	wetted area
P	wetted perimeter
N_R	total number of fractures in the reservoir
N_R	number of fractures on each row on the reservoir inlet face
C_P	specific heat capacity of the fluid (J/kg/K)
W_R	width of the reservoir
ρ	density of the fluid in the reservoir (kg/m^3)
Pr_f	Prandtl number evaluated at the average fluid temperature
Pr_w	Prandtl number evaluated at the reservoir wall temperature
U	Overall heat transfer coefficient ($W/m^2/K$)
Bi	Biot number
$T_{R,t}$	temperature of the geothermal rock at any time t (K)
$T_{F,0}$	temperature of the fluid at the inlet of the geothermal reservoir in the bottom of the injection well (K)
$Q_{R,t}$	heat contained in the geothermal reservoir at time t (J)
t	time of geothermal reservoir degradation (yr)
D_H	hydraulic diameter (m)
m_f	mass flow rate per unit fracture
Re	Reynolds number
Pr	Prandtl number
Nu	Nusselt number
μ	viscosity of the fluid (kg/m/s/)
k	thermal conductivity of the fluid (W/m/K)
k_S	thermal conductivity of the rock (W/m/K)
h	heat transfer coefficient (W/m/K)
C_{PR}	specific heat capacity of the rock (J/kg/K)
Q_{GEO}	rate of geothermal heat energy absorption (W)
A_F	heat transfer area in the fractures (m^2)
β	volumetric coefficient of expansion of the fluid (K^{-1})
Ra'	channel Rayleigh number for constant surface temperature
h	convective heat transfer coefficient ($W/m^2/K$)
A_H	heat transfer area per unit fracture (m^2)
$T_{R,0}$	initial temperature of the geothermal rock (K)
$T_{R,t+1}$	temperature of the geothermal rock at any time $(t+1)$ (K)
$Q_{R,t+1}$	heat contained in the geothermal reservoir at time $t+1$ (J)
ΔQ	amount of heat absorbed by CO_2 flowing through a fracture slice in a certain interval of time (t)

clearly shows that geothermal energy is yet to be utilized to its full potential in the United States (Duchane, 1996). Modeling studies show that the amount of recoverable geothermal energy for a stimulated rock volume of 0.1 km^3 is 40% for a range of well geometries, fracture spacing and permeabilities (Sanyal and Butler, 2005). The magnitude of stimulated rock volume in the EGS reservoirs ranges from 0.5 km^3 to 3 km^3 (The Future of Geotherrmal Energy, 2006). For a stimulated rock volume of 2.7 km^3, the amount of power that can be generated in EGS is estimated to be 50 MW_e (The Future of Geotherrmal Energy, 2006).

Conventional EGS uses water as a circulating fluid for the extraction of the geothermal heat energy. Geothermal source temperatures, reservoir conditions like porosity, permeability etc and the well head pressure determine the quality of the hot water, or more typically brine, or steam generated. The quality of the working fluid determines the type of plant used downstream for power generation (DiPippo, 1999). The Geysers in northern California is a rare example where a dry steam plant is used for the conversion of geothermal energy into electricity (Mock et al., 1997). In the case of a two phase mixture, steam is separated from the high-pressure liquid water in the mixture in a pressurized vessel and expanded in a high-pressure turbine in single-flash plants. Throttling of the high-pressure liquid water produces low-pressure steam that generates 20% to 30% of additional power upon expansion in a low-pressure turbine in double-flash steam plants, compared to single-flash steam plants (DiPippo, 1999).

2. Utilization of supercritical CO_2 as a heat transfer fluid for geothermal heat absorption

There are arid regions especially in the southwestern part of the United States, where geothermal energy is abundant in the form of high-enthalpy heat (The Future of Geotherrmal Energy, 2006; Blackwell and Richards, 2004) but that have an acute shortage of water. In these regions, there is a necessity to replace water with a fluid like CO_2 that is available in large quantities at an affordable cost whose removal from the atmosphere is necessary to prevent global warming. The total amount of CO_2 emitted from the coal-fired power plants in the United States in 2012 was 1.72 Gt (US Carbon, 2012). Sequestration of CO_2 may become mandatory in the future to mitigate global warming (Kramer, 2012). Deep saline aquifers and depleted hydrocarbon fields were the only known sequestration sites for CO_2 emitted from the power plants (Bachu, 2008). Another alternative is to use CO_2 as a geothermal heat transfer fluid for the simultaneous extraction of geothermal heat energy and sequestration of CO_2 (Randolph and Saar, 2011a). Among the various geothermal resources, sedimentary rock formations and crystalline basement rock formations that are conduction-dominated are potential sites for enhanced geothermal systems (EGS). The amount of geothermal energy stored in sedimentary rock formations and in crystalline basement rock formations are 100,000 EJ and 13 million EJ, respectively (The Future of Geotherrmal Energy, 2006). Natural high permeability formations referred to as CO_2-plume geothermal (CPG) are much larger than the low permeability formations and they do not need external stimulation by hydraulic fracturing (Randolph and Saar, 2011b). As the intrinsic permeability of these rocks comprising the geothermal reservoir in the conventional enhanced geothermal systems (EGS) is very low typically in the micro-Darcy range, stimulation of the low permeability rocks is necessary in such systems. This may be accomplished by hydraulic fracturing or hydraulic shearing to create new fractures, improve the network between existing fractures to expand the site of the reservoir, elevate the permeability and thus the fluid flow-through rates, increase the heat transfer area between the reservoir fluid and the rocks, and increase the connectivity between the injection wells and the production wells.

There are four trapping mechanisms that determine the storage density and leakage potential of any geological sink used for CO_2 sequestration (Nelson et al., 2005; White et al., 2003). Solubility trapping is predominant in enhanced oil recovery (EOR) where

Table 1
Ultimate analysis of Illinois no 6 coal on a dry basis.

Elements	Composition (%)
Carbon	65.65
Hydrogen	4.23
Nitrogen	1.16
Sulfur	4.83
Oxygen	8.60
Chlorine	0.03
Ash	15.48

CO_2 is soluble in immobile, non-recoverable fraction of crude oil or in porous water-filled rock layers capped by an impermeable rock layer where CO_2 is trapped by its dissolution in water as carbonic acid or aqueous carbonates (White et al., 2003). Hydrodynamic trapping is predominant in the free pore space of a porous rock layer capped by an impermeable rock (White et al., 2003). Adsorption trapping is predominant in coal seams and shales where higher hydrostatic pressure facilitates the adsorption of CO_2 on the micropore surfaces coal organic matter, kerogens or minerals (White et al., 2003). In sandstone aquifers low in carbonate rocks and rich in minerals like illite, smectite anorthite and other chlorites, the chemical reaction between Ca, Mg and Fe in these minerals and dissolved CO_2 (White et al., 2003).

There are three leakage mechanisms through which CO_2 reaches the surface escaping the geological sink. If the casings are sealed properly, CO_2 leaks through the transmissive faults or fractures through the cap rocks, loss of dissolved CO_2 due to the hydrodynamic flow of formation water from the geological sink and the desorption of adsorbed-phase CO_2 (Nelson et al., 2005).

Typically water and brine are used as heat transfer fluids for the extraction of geothermal heat energy (DiPippo, 1999). Instead of treating CO_2 as a waste pollutant from the power plant that is in need of disposal through sequestration in a geological site, the concept of using CO_2 as a heat transfer fluid for the extraction of geothermal heat energy had been proposed earlier (Randolph and Saar, 2011b; Brown, 2000; Pruess, 2006, 2008; Pritchett, 2009). While the specific heat capacity of supercritical CO_2 is less than that of water, the fluid mobility (density/viscosity) for supercritical CO_2 is greater than that of water permitting 60% higher heat extraction from the geothermal reservoir with supercritical CO_2 as the heat transfer fluid (Brown, 2000; Pruess, 2008; Atrens et al., 2010). When exposed to minerals in the fractures in the geothermal reservoir, the solubility of minerals in non-polar CO_2 under supercritical condition is very low compared to that in water (Brown, 2000). Therefore, corrosion is reduced in the wellbore piping and on the surface equipment. The larger expansivity and compressibility of supercritical CO_2 enhances the buoyancy effect (Atrens et al., 2010; Atrens et al., 2009) of CO_2 between the injection and the production well, leading to self-driven high flow rates (Atrens et al., 2010) and reducing the power consumption for the geothermal fluid recirculation (Pruess, 2006). To produce the same amount of electricity, the temperature of a geothermal reservoir using CO_2 as a heat transfer fluid can be lower than the traditional water-based geothermal reservoir (Randolph and Saar, 2011a). Reservoir modeling studies for CO_2-EGS system have shown that the significant portion of the pressure drop across the geothermal reservoir is concentrated in regions near injection wells and production (Atrens et al., 2010). Increasing the CO_2 injection pressure, increases the pressure drop across the production well, thereby increasing the entropy (Atrens et al., 2010). The exergy of CO_2 in the production well surface reaches a maximum and then subsequently decreases with the increasing injection pressure (Atrens et al., 2010). With Sc CO_2 as a geothermal heat extraction fluid, the pressure drop along the production well is higher than that across the reservoir (Atrens et al., 2010). Preliminary calculations have shown that, with CO_2 as a geothermal heat extraction fluid in EGS, for every megawatt of electricity generated by EGS, the amount of CO_2 necessary for EGS has to come from a 3 MW_e coal-fired power plant (Pruess, 2006). At such high consumption rates, pairing a coal fired power plant with EGS may facilitate the simultaneous extraction of geothermal heat energy and sequestration of CO_2 (Frank et al., 2012).

Table 2
Analysis of CO_2 emissions from three power generation technologies.

	Sub-critical	Oxy-combustion	IGCC
Electrical Output (MW_e)	629	629	629
Efficiency (% HHV)	35	38	42
Thermal input (MW_{th})	1797	1655	1498
Calorific value of fuel HHV (kJ/kg)	27,800	27,800	27,800
Coal needed (kg/s)	64.6	59.5	53.9
Carbon in coal from ultimate analysis (kg/s)	39.6	36.4	32.9
CO_2 emitted (kg/s)	145	134	120
Discharge pressure of CO_2 (MPa)	0.1	0.1	15

3. Selection of a CO_2 source for pairing with EGS

A 629 MW_e coal-fired power plant is chosen as the basis for this study. A conventional subcritical air-blown coal-fired power plant and two potential technologies oxy-combustion and integrated gasification combined cycle (IGCC), are considered as sources for the CO_2. It is assumed that Illinois no 6 coal, whose ultimate analysis is given in Table 1, is chosen for power generation. Table 2 shows the basis for the calculations, the amount of CO_2 obtained from each plant, and the conditions under which CO_2 is captured from the power plant. The temperature and pressure of CO_2, available from a coal-fired power plant for geological sequestration, decides symbiotic nature of pairing carbon capture and storage (CCS) with geo-thermal energy extraction (Brown, 2000; Rubin et al., 2012). Among the three technologies, subcritical pulverized coal combustion, oxy-combustion (Buhre et al., 2005) and coal-based integrated gasification combined cycle (IGCC) that are available for power generation, subcritical pulverized coal combustion is not suitable due to enormous amounts of energy consumed in the separation of CO_2 followed by compression from atmospheric pressure to the sequestration pressure after its capture (Figueroa et al., 2008). Similarly, in oxy-coal combustion power generation method, even though a separate technology is not necessary for carbon capture due to the use of oxygen with 95% purity (Pruess, 2008), it is not advantageous to pair with EGS due to the energy involved in the compression of CO_2 from atmospheric pressure to sequestration pressure. In IGCC, operating the gasification reactor during the transformation of carbonaceous feedstock at high pressure (3 MPa) facilitates the removal and capture of CO_2 at high pressures as mentioned in Table 2 and minimizes the energy spent in the compression of CO_2 to the sequestration pressure (15 MPa). Thus, a high pressure gasification process, followed by pre-combustion carbon capture makes the IGCC–EGS pair, a symbiotic combination for the simultaneous sequestration of CO_2 and the absorption of geothermal heat energy.

4. Modeling assumptions used in the study

This paper focuses on modeling the utilization of CO_2 intended for sequestration from an IGCC plant as a heat transfer fluid for extraction of geothermal energy in an EGS and using it for additional power generation. The numerical modeling is conducted in ASPEN Plus V7.3 (Brown, 2000). Fig. 1a shows a flowchart that gives the pathway followed by supercritical CO_2 for the simultaneous

extraction of geothermal heat energy for electricity generation by EGS and sequestration of CO_2 emitted from a 629 MW_e IGCC plant. Fig. 1b shows the schematic of our modeling methodology that was adopted for analysis. It is assumed that 10% of the total CO_2 injected into the geothermal reservoir is lost in the fractures and contribute to the sequestration process. This CO_2 loss is compensated by CO_2 coming from the 629 MW_e IGCC plant. Table 2 shows that that this plant captures 120 kg/s of CO_2 for sequestration at a pressure of 15 MPa and 60 °C. CO_2 leaving the IGCC plant for sequestration is under supercritical condition. This amounts to 10% of the total CO_2 injection rate which is 1200 kg/s. From Fig. 1a, it can be seen that the total injection rate of 1200 kg/s of CO_2 is distributed equally among 10 blocks. Each block is assumed to be made up of an injection well, geothermal reservoir and a production well connected with one another receiving 120 kg/s of CO_2 at the inlet of the injection well and discharging 108 kg/s of CO_2 at the outlet of the production well after a loss of 10% in the reservoir. This configuration is shown in the schematic in Fig. 1b. Each block is assumed to repeat itself adjacent to one another. The distance between each reservoir block is equal to the length of the reservoir mentioned in Table 4. As the blocks are exactly identical to one another in all aspects, further description about the modeling of the system will be centered on the wells and the reservoir in a block. Fig. 1a shows that the CO_2 is accumulated from the outlet of all the 10 production wells on the surface before entering the EGS section for electricity generation. Fig. 1b shows the schematic of the configuration of the EGS to utilize both the pressure energy and the geothermal energy of the 1080 kg/s of supercritical CO_2 from the outlet of the production well for electricity generation.

Table 3
Properties of the rock in the geothermal reservoir (The Future of Geotherrmal Energy, 2006).

Specific heat capacity of the rock (J/kg/K)	1000
Density of the rock (kg/m^3)	2550
Ambient temperature (K)	313
Thermal conductivity of the rock (W/m/K)	2
Project life (years)	25

5. Injection well

It is assumed that the total Sc CO_2 injection rate of 1200 kg/s is distributed equally among 10 injection wells and extracted equally from 10 productions wells. The first part of modeling simulates the pressure and temperature profile of the supercritical CO_2, i.e., Sc CO_2, along the injection well. The injection well comprises three pipe sections connected to one another in series to transfer Sc CO_2 to the reservoir inlet. The first well section has an inner diameter of 0.445 m (17.5 in.) and is 3048 m long (Polsky, 2008). The second well section has an inner diameter of 0.3175 m (12.5 in.) and is 2133 m long (Polsky, 2008). The third section has an inner diameter of 0.2159 m (8.5 in.) and is 914 m long (Polsky, 2008). The total depth of an injection well is 6095 m. The injection well is assumed to be an open pipe without perforations.

Table 4
Geothermal reservoir characteristics and fracture dimensions.

Stimulated volume			Permeability (mD)	Fracture spacing (m)	Fracture width (mm)	Porosity	Fracture dimensions			
L_R (km)	W_R (km)	H_R (km)					L (km)	W (mm)	H (m)	Total fractures
0.5	0.5	0.5	100	10	0.23	2.3×10^{-5}	0.5	0.23	500	50
0.5	0.5	0.5	100	50	0.39	7.8×10^{-6}	0.5	0.39	500	10
1	1	1	100	10	0.23	2.3×10^{-5}	1	0.23	1000	100
1	1	1	100	50	0.39	7.8×10^{-6}	1	0.39	1000	20
1.58	1	1.58	100	10	0.23	2.3×10^{-5}	1	0.23	1581	158
1.58	1	1.58	100	50	0.39	7.8×10^{-6}	1	0.39	1581	32
1.58	1	1.58	10	50	0.18	3.6×10^{-6}	1	0.18	1581	32

Table 5a
Variation in the high pressure turbine power output with Sc CO_2 as a primary working fluid during the thermal degradation of low temperature geothermal reservoir.

Reservoir characteristics—2.5 km^3, 10 mD and 50 m fracture spacing. Initial T_{GEO} = 200 °C					
Time (yr)	Production well outlet		High pressure gas turbine (HPGT) output		
	T_{CO_2} (K)	P_{CO_2} (MPa)	T_{CO_2} (K)	P_{CO_2} (MPa)	Power (MW_e)
0	406	24.1	372	15	18
5	395	23	365	15	15
10	381	21.5	358	15	11
15	368	19.9	351	15	8
20	357	18.4	346	15	5
25	349	17.2	342	15	3

Table 5b
Variation in the high pressure turbine power output with Sc CO_2 as a primary working fluid during the thermal degradation of high temperature geothermal reservoir.

Reservoir characteristics—2.5 km^3, 10 mD and 50 m fracture spacing. initial T_{GEO} = 300 °C					
Time (yr)	Production well outlet		high pressure gas turbine (HPGT) output		
	T_{CO_2} (K)	P_{CO_2} (MPa)	T_{CO_2} (K)	P_{CO_2} (MPa)	Power (MW_e)
0	511	31.3	448	15	44
5	486	30	428	15	38
10	454	28	404	15	30
15	422	25.6	382	15	22
20	394	22.9	365	15	15
25	373	20.6	354	15	9

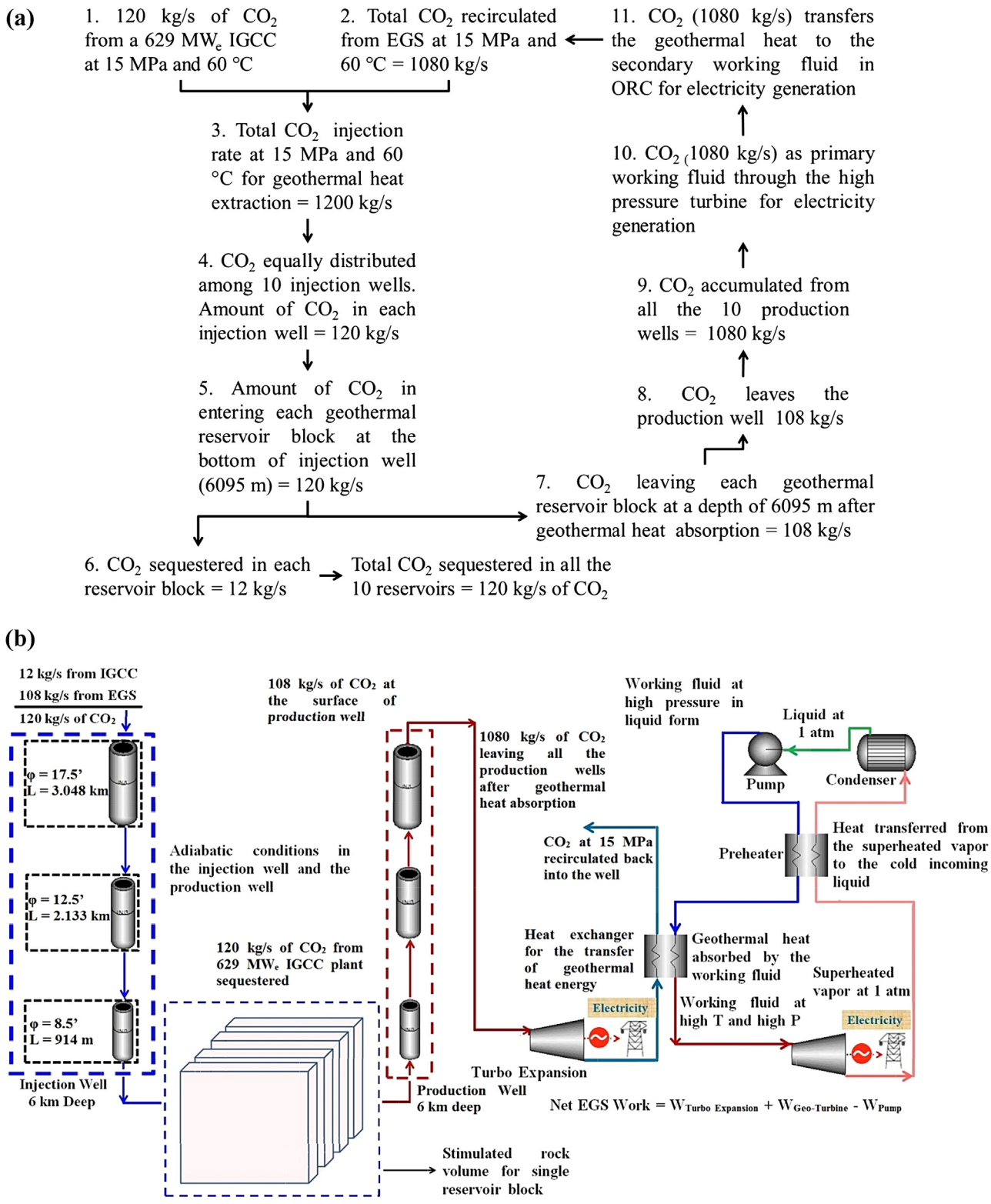

Fig. 1. (a) Flowchart showing the CO_2 utilization pathway for the simultaneous extraction of geothermal heat energy and sequestration of CO_2. (b) Schematic representation of the geothermal heat utilization in each block for power generation.

6. Stimulated geothermal reservoir volume

The reservoir is located at the bottom of the injection well at a depth of 6095 m at the bottom of the injection well. Table 3 summarizes the thermophysical properties of the rock used in the heat transfer calculations to calculate the rock surface temperature and the Sc CO_2 temperature at the geothermal reservoir outlet over a period of 25 years (The Future of Geotherrmal Energy, 2006). Table 4 summarizes the reservoir parameters such as stimulated rock volume, permeability of the reservoir and the fracture spacing used as assumptions to derive the porosity and fracture dimensions corresponding to the reservoir geometry for use in the heat

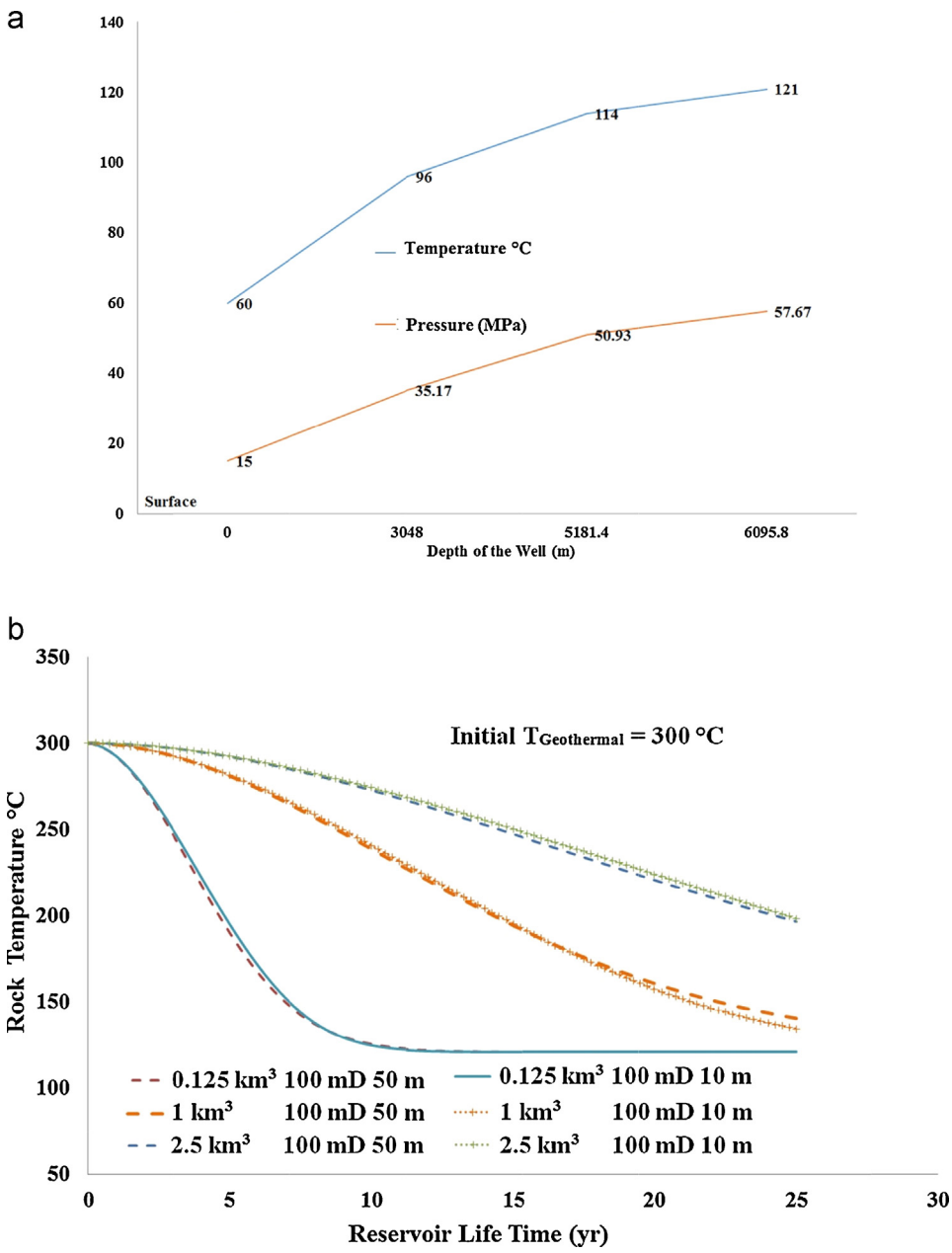

Fig. 2. (a) Temperature and pressure profiles of CO_2 along the injection well. (b) Thermal degradation profiles of different geothermal reservoirs initially at 300 °C at a depth of 6 km over a period of 25 years.

transfer calculations in the second part of analysis. Based on the assumptions, the dimensions of the fracture and total void volume are calculated using Eqs. (1)–(8) and given in Table 4. The fractures are assumed to be narrow vertical channels. The amount of Sc CO_2 flowing through each injection well is 120 kg/s. This is distributed equally among all fractures in the stimulated reservoir. For each reservoir condition, two geothermal sources one at 200 °C and the other at 300 °C are considered. The thermal and hydrodynamic properties of the Sc CO_2 are evaluated using REFPROP model for each time interval (t = 0.25 yr) in ASPEN Plus at the average temperature between Sc CO_2 at the bottom of the injection well (121 °C) and the geothermal reservoir at that time. Based on the fracture dimensions in Table 4, the hydraulic diameter is calculated using Eqs. (9)–(11). The hydraulic diameter of the rectangular channel is used to characterize the flow of Sc CO_2 through the fracture. Smaller fracture spacings of 10 m in a reservoir increase the number of fractures per unit reservoir volume and decrease the mass flow rate per unit fracture. For such cases, the reservoir can be assumed to be at a constant temperature and the convective heat transfer coefficient was found by the empirical correlations given by Eqs. (15) and (16) that are used typically for heat transfer in channels with a very high aspect ratio (Atrens et al., 2010). Larger fracture spacings of 50 m in a reservoir decrease the number of fractures per unit reservoir volume and increase the mass flow rate per unit fracture. For such cases, a constant heat flux is assumed to exist between the rock of the reservoir and the fluid in each fracture and the convective heat transfer coefficient was found by the Collier empirical correlation given by Eq. (17) (Atrens et al., 2009). The convective heat transfer coefficient is derived from the Nusselt number using Eq. (18). By combining the convective heat transfer coefficient and the thermal conductivity of the rock, the overall heat transfer coefficient is calculated with the help of Eqs. (19)–(21). The Biot number, defined as the ratio of heat transfer by convection to heat transfer by conduction, calculated by Eq. (21) is less than 0.1 for all the

Table 6a
Total net power output from EGS for five different working fluids over 25 years from a geothermal reservoir of volume 2.5 km^3, 10 mD and 50 m fracture spacing initially at 200 °C.

Time (yr)	Working fluid	Mass flow (kg/s)	Pressure (MPa)	Preheating (Q) (%)	ORC power output (MW_e)	η (%)	Total net EGS output (MW_e)
0	Isobutane	350	0.5	2	18.9	10.1	36.9
	Ammonia	115	0.5	0	19.1	10	37.1
	n-Butane	350	0.5	3	18.8	10	36.8
	Neopentane	425	0.5	3.5	18.3	9.7	36.3
	Isopentane	425	0.5	2.5	17.9	9.5	35.9
5	Isobutane	325	0.6	0	18.7	10.9	33.7
	Ammonia	105	0.5	0	17.2	10	32.2
	n-Butane	325	0.8	0	20.8	12.1	35.8
	Neopentane	400	0.8	0	20.2	11.8	35.2
	Isopentane	385	0.4	0	14	8.2	29
10	Isobutane	325	0.6	10	18.3	12	29.3
	Ammonia	95	0.45	0	14.2	9.3	25.2
	n-Butane	325	0.5	10	16.4	11	27.4
	Neopentane	375	0.5	0	14.7	9.6	25.7
	Isopentane	375	0.3	0	10.3	6.7	21.3
15	Isobutane	280	0.75	5	16.6	12.6	24.6
	Ammonia	82.5	0.4	0	11.2	7.4	19.2
	n-Butane	280	0.5	7.5	14	10.5	21.9
	Neopentane	325	0.5	0	12.6	9.6	20.6
	Isopentane	325	0.2	0	5.7	4	13.7
20	Isobutane	250	0.6	7.5	13.4	9.8	18.4
	Ammonia	72.5	0.35	0	8.9	7.8	13.9
	n-Butane	225	0.3	0	8	6.9	13
	Neopentane	275	0.4	0	9.7	8.4	14.7
	Isopentane	275	0.3	0	7.7	6.7	12.7
25	Isobutane	225	0.6	5	11.4	11.5	14.4
	Ammonia	65	0.3	0	6.7	6.6	9.7
	n-Butane	225	0.3	5	7.3	7.3	10.3
	Neopentane	250	0.25	0	5.8	5.8	8.8
	Isopentane	250	0.25	0	5.7	5.7	8.7

cases considered in this study suggesting that external resistance to heat transfer between the rock of the reservoir and the Sc CO_2 is far greater than the internal resistance to heat transfer within the reservoir (Frank et al., 2012). Therefore, the decreasing temperature of the reservoir due to the geothermal heat absorption by Sc CO_2 is estimated by lumped parameter analysis in the interval of every three months (t = 0.25 yr) by Eq. (22) over a period of 25 years. The amount of heat absorbed by Sc CO_2 in a certain time interval is calculated using Eqs. (23)–(25). Based on the amount of heat absorbed corresponding to the reservoir temperature at each time interval,

Table 6b
Total net power output from EGS for four different working fluids over 25 years from a geothermal reservoir of volume 2.5 km^3, 10 mD and 50 m fracture spacing initially at 300 °C.

Time (yr)	Working fluid	Mass flow (kg/s)	Pressure (MPa)	Preheating (Q) (%)	ORC power output (MW_e)	η (%)	Total net EGS output (MW_e)
0	Isobutane	600	2.7	20	66.6	20.8	110.9
	n-Butane	600	1.3	15	52.4	16.4	96.7
	Neopentane	575	1.2	10	44.6	13.9	88.9
	Isopentane	575	1.2	5	42.7	13.3	87
5	Isobutane	550	2.5	17.5	58	20	96
	n-Butane	550	1.4	15	48.6	16.7	86.6
	Neopentane	525	0.8	5	34	11.6	72
	Isopentane	525	1.2	2.5	38	13.1	76
10	Isobutane	495	2	12.5	45.8	18.2	75.8
	n-Butane	475	1.2	12.5	39.2	15.6	69.2
	Neopentane	475	0.6	0	25	9.97	55
	Isopentane	495	1	0	30.9	12.3	60.9
15	Isobutane	430	1.4	10	34.3	16.3	56.3
	n-Butane	400	0.9	7.5	28.5	13.6	50.5
	Neopentane	475	0.6	7.5	23	10.9	45
	Isopentane	450	0.7	0	22.8	10.9	44.8
20	Isobutane	325	0.6	0	18.7	10.9	33.7
	n-Butane	325	0.8	0	20.8	12.1	35.8
	Neopentane	400	0.8	0	20.2	11.8	35.2
	Isopentane	385	0.4	0	14	8.2	29
25	Isobutane	300	0.85	5	18.7	13.3	27.7
	n-Butane	300	0.55	5	15.1	10.8	24.1
	Neopentane	325	0.3	0	9.4	6.7	18.4
	Isopentane	325	0.3	0	9.3	6.6	18.3

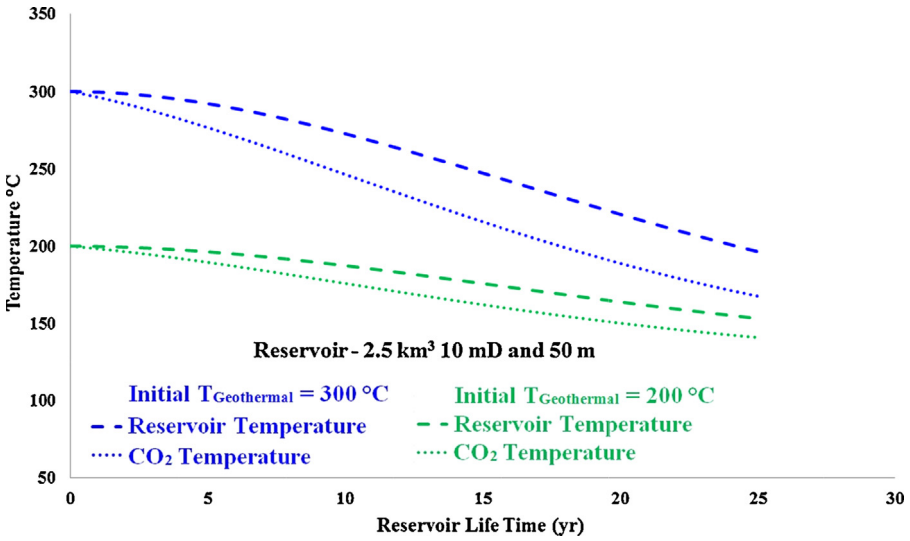

Fig. 3. Thermal degradation profiles of two geothermal reservoirs at a depth of 6 km and CO_2 temperature at the respective reservoir outlets over a period of 25 years.

the temperature of Sc CO_2 in the outlet of the geothermal reservoir at the bottom of the production well is calculated by Eq. (26). Based on the temperature profile of different reservoir geometries over a period of 25 years, a reservoir of volume 2.5 km^3, permeability of 10 mD and fracture spacing of 50 m is used for subsequent calculations discussed below.

7. Production well

For reservoirs with a volume of 0.125 km^3, the distance between the injection well and the production well is 500 m. For other reservoirs, it is 1000 m. The production well also has three pipe sections whose length and diameter are the same as for the injection well. Adiabatic conditions are assumed in both the injection and production wells. The temperature and pressure of Sc CO_2 at which it leaves the reservoir and enters the bottom of the production well at different time periods for two geothermal source temperatures 200 °C and 300 °C, respectively serve as inputs in ASPEN Plus to obtain the temperature and pressure profiles of Sc CO_2 along the entire length of the production well. The temperature and pressure of Sc CO_2 at the outlet of the production well for the two geothermal source temperatures 200 °C and 300 °C are tabulated in Tables 5a and 5b, respectively.

8. Organic Rankine cycle (ORC)

The organic Rankine cycle can be suitable for the utilization of low-grade heat energy to produce lower-capacity decentralized electrical energy. ORC is typically used for the utilization of thermal energy from solar ponds, geothermal energy (Rubin et al., 2012), industrial waste heat, and biomass combined waste heat and power (Chen et al., 2010). The minimum temperature of the heat source should be above 80 °C so that the conversion efficiency is substantial to make the geothermal plant operate economically, although lower temperature may also be utilized economically, particularly when Sc CO_2 is used as the sub-surface heat extraction working fluid (Quoilin et al., 2013; Adams et al., 2014). In ORCs that are typically used in the geothermal power plants, brine transfers the geothermal heat energy in the evaporator heat exchanger to working fluid in the ORC. Previous studies have shown that when Sc CO_2 is used as a heat transfer fluid, the pressure of Sc CO_2 in the production well outlet always exceeds the injection pressure (Randolph and Saar, 2011a; Pruess, 2006; Adams et al., 2014). As Sc CO_2 is used as a heat transfer fluid in this study, the ORC is modified to utilize both the pressure energy and temperature of Sc CO_2 in electricity generation (Adams et al., 2014). Fig. 1 shows the modification of the ORC used in this study. The Sc CO_2 leaving the production well is recirculated back after the extraction of geothermal energy by the ORC. As the pressure of CO_2 leaving the production well is significantly higher than the injection pressure of 15 MPa, it is expanded as a primary working fluid through the high-pressure turbine to the injection pressure of 15 MPa extracting work for the generation of electricity. The temperature of Sc CO_2 after the expansion is greater than 60 °C. Therefore, the balance geothermal heat energy is transferred to the secondary working fluid used in the ORC. This is accomplished by pumping the secondary working fluid to high pressure before it enters the heat exchanger. The geothermal heat is transferred from Sc CO_2 to the secondary working fluid. The mass flow rate of the secondary working fluid is such it transitions completely to its vapor phase at the outlet of the heat exchanger and is sufficiently superheated before entering the inlet of the turbine to avoid the formation of liquid droplets during the expansion process in the turbine. Expansion of the secondary working fluid through the turbine to atmospheric pressure produces electricity. The hot vapor leaving the turbine has sensible heat. This heat can be transferred to the incoming cold high-pressure liquid in a preheater or recuperator. The working fluid in the liquid state at atmospheric pressure is recirculated from the condenser to the pump to form a closed loop.

The secondary working fluids chosen for the ORC are expected to have low dynamic viscosity to reduce the frictional losses, high thermal conductivity, lower global warming potential and lower ozone depletion potential (Quoilin et al., 2013). The fluid should also have stability at high temperature to prevent thermally induced decomposition of hydrocarbons (Quoilin et al., 2013). These factors determine the choice of fluid used in the ORC for a certain source temperature (Quoilin et al., 2013). Extensive studies have been conducted on the properties of working fluid that are suitable for the organic Rankine cycle (Aljundi, 2011; Edrisi and Michaelides, 2013; Liu et al., 2004; Schuster et al., 2010; Bruhn, 2002; Madhawa Hettiarachchi et al., 2007; Brasz and Bilbow, 2004; Guo et al., 2011; Sotirios and Andreas, 2010; Lai et al., 2011; Saleh et al., 2007; Heberle et al., 2012). The working fluids used in the ORC are categorized into three different types depending upon the slope of the vapor saturation curve in the *T–S* diagram (Aljundi,

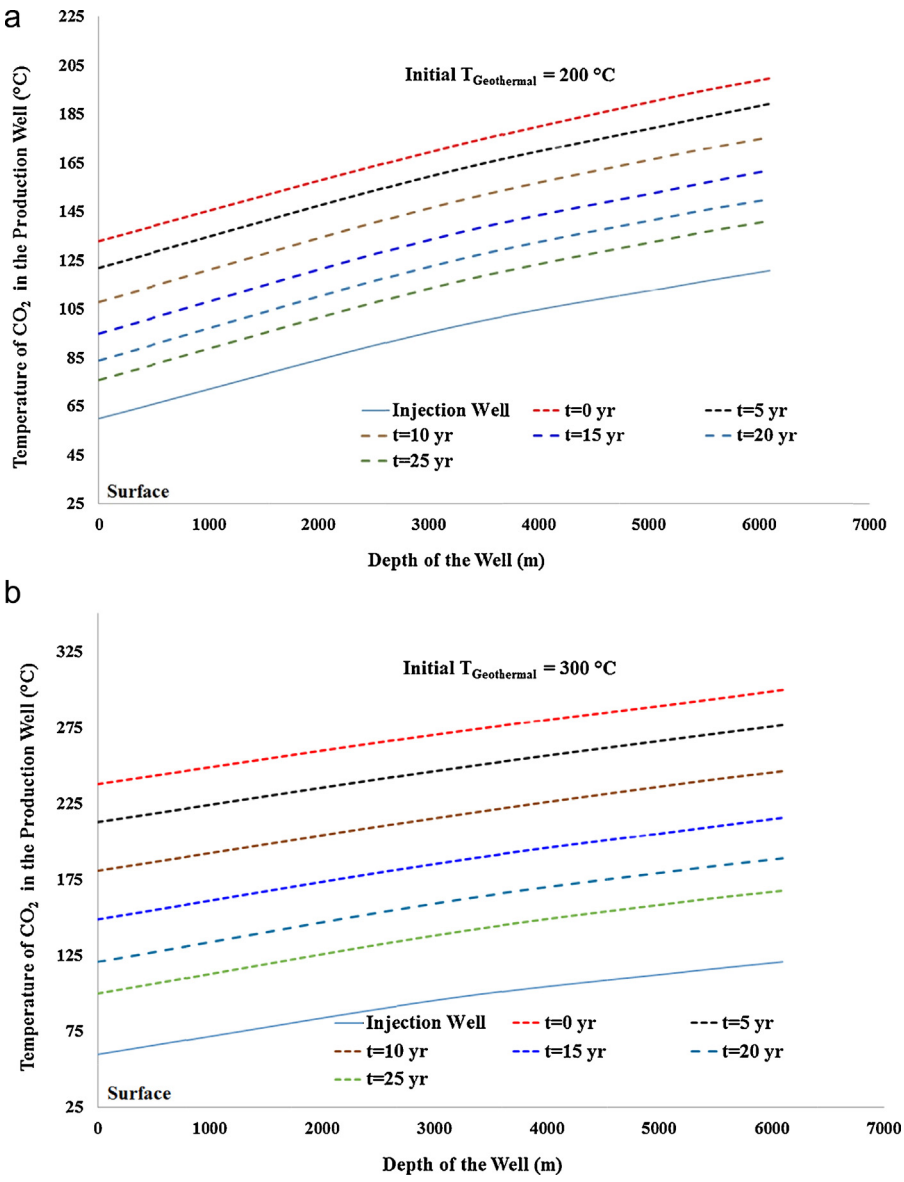

Fig. 4. (a) Temperature profile of CO_2 in the injection well and production well for 25 years from a geothermal reservoir 2.5 km^3, 10 mD and 50 m fracture spacing at 200 °C initially. (b) Temperature profile of CO_2 in the injection well and production well for 25 years from a geothermal reservoir 2.5 km^3, 10 mD and 50 m fracture spacing at 300 °C initially.

2011). The slope of the vapor saturation curve is negative for wet fluids and positive for dry fluids (Aljundi, 2011). Isentropic fluids have infinitely large positive slope (Aljundi, 2011). In the case of dry fluids, the fluid is in superheated state after expansion to atmospheric pressure through the turboexpander. Presence of a recuperator before the condenser facilitates the extraction of sensible heat energy from the superheated vapor in the case of dry fluids. Presence of hydrogen bonds in the secondary working fluids increases the enthalpy of vaporization for wet fluids like ammonia and water. Below a certain source temperature, expansion of a wet fluid through the turbine can cause condensation that can harm the turbine blades. Therefore, the temperature of the fluid at the turbine inlet determines its suitability in the ORC. In this study neopentane, isopentane, *n*-butane and isobutane are the four secondary working fluids chosen for the utilization of high-enthalpy heat. Ammonia is chosen as a wet tertiary working fluid for the utilization of low-enthalpy heat.

9. Results and discussion

9.1. Injection well

The temperature and pressure profiles of Sc CO_2 flowing through the injection well is independent of the geothermal source temperature and is shown in Fig. 2a. The temperature profile of Sc CO_2 is non-linearly increasing from 60 °C to 121 °C at a depth of 6095 m. Even though, adiabatic conditions are assumed in the simulation, compression of the fluid to high pressures increases the temperature of Sc CO_2. The increase in temperature of Sc CO_2 shown in this simulation is significantly higher than that observed for water (Pruess, 2006). The pressure of Sc CO_2 increases from the sequestration pressure of 15 MPa to 58 MPa as it flows from the surface to a depth of 6095 m. Gravitation, deceleration of the fluid, while descending along the injection well, and frictional losses along the well casings of different diameters, determine the pressure of Sc CO_2 from the surface to the bottom of the injection well. The

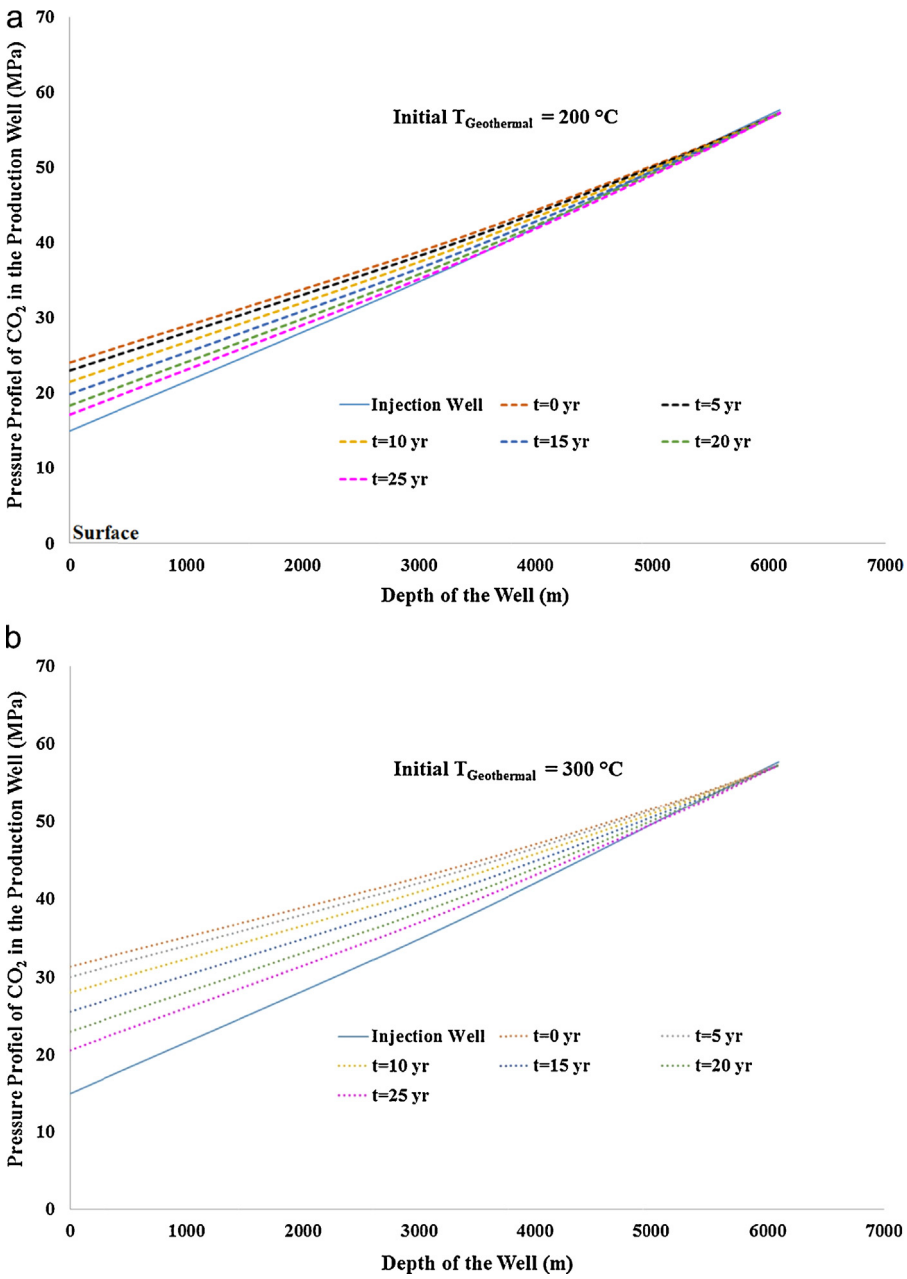

Fig. 5. (a) Pressure profile of CO_2 in the injection well and production well for 25 years from a geothermal reservoir 2.5 km^3, 10 mD and 50 m fracture spacing at 200 °C initially. (b) Pressure profile of CO_2 in the injection well and production well for 25 years from a geothermal reservoir 2.5 km^3, 10 mD and 50 m fracture spacing at 300 °C.

contribution of gravitation to the increase in pressure is substantially higher than the other two factors.

9.2. Stimulated rock volume

The temperature and pressure of Sc CO_2 at the bottom of the injection well is 121 °C and 57.67 MPa, respectively, and therefore enters the reservoir inlet at supercritical conditions. Fig. 2b shows the thermal degradation of different geothermal reservoirs described in Table 4 over a period of 25 years. It shows that larger reservoir volume is necessary to sustain the heat mining process for a longer duration of time. For a reservoir volume of 0.125 km^3, the reservoir temperature decreases from 300 °C to 121 °C within a period of 10 years. Increasing the reservoir volume to 1 km^3 lowers the rate of depletion of geothermal energy and decreases the temperature of the reservoir from 300 °C to 132 °C over a period of 25

Table 7
Time-averaged net EGS power output (MW_e) from a geothermal reservoir 2.5 km^3, 10 mD and 50 m fracture spacing over a period of 25 years.

Initial T_{GEO} (°C)	Time-averaged net EGS power output (MW_e)				
	Isobutane	*n*-Butane	Ammonia	Neopentane	Isopentane
200	21	17	16	17	14
300	46	43		37	36

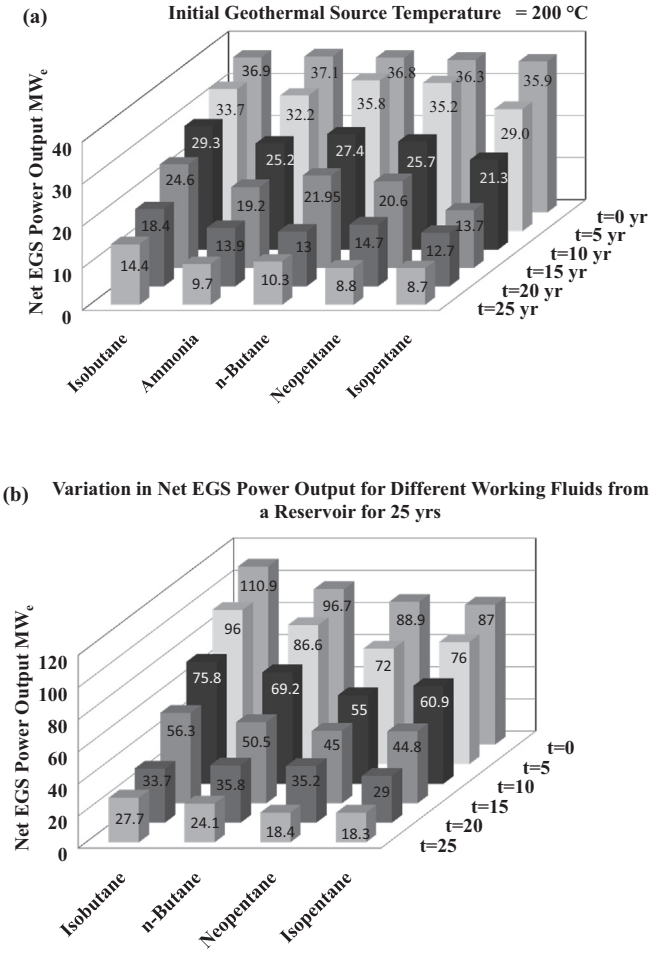

Fig. 6. (a) Net EGS power output for five different secondary working fluids from a geothermal reservoir of volume 2.5 km^3, 10 mD, 50 m spacing at an initial geothermal source temperature of 200 °C. (b) Net EGS power output for five different secondary working fluids from a geothermal reservoir of volume 2.5 km^3, 10 mD, 50 m spacing at an initial geothermal source temperature of 300 °C.

years. When the mass flow rate of Sc CO_2 injected into the geothermal reservoir is 120 kg/s, increasing the reservoir volume to 2.5 km^3 substantially decreases the rate of depletion of geothermal energy and significantly improves the longevity of the reservoir. The rate of decrease in temperature is approximately 4 °C per year for a reservoir volume of 2.5 km^3. Over a period of 25 years, the reservoir temperature decreases to 198 °C facilitating the extraction of geothermal energy for the sustained production of electricity. For any stimulated rock volume with a fixed permeability, wider fracture spacings decrease the porosity and hence the total number of fractures with larger hydraulic diameter for each fracture on the reservoir inlet (face of the cubical block where fluid enters for absorbing the geothermal energy). Each fracture is modeled as a narrow rectangular channel. Reynolds number calculated based on the hydrodynamic conditions shows that the flow of the fluid is laminar through each fracture for all the reservoir geometries. Lower permeability increases the pressure drop of Sc CO_2 across the reservoir. Based on the thermal degradation of a geothermal reservoir over a period of 25 years, a reservoir of volume 2.5 km^3 with a permeability of 10 mD and a fracture spacing of 50 m is chosen for a detailed study of extraction of geothermal energy for electricity generation by organic Rankine cycle in enhanced geothermal systems.

Fig. 3 shows the thermal degradation of a geothermal reservoir and the corresponding Sc CO_2 temperature at the reservoir outlet, respectively, for a reservoir of volume 2.5 km^3, 10 mD and 50 m fracture spacing over a period of 25 years that was initially at 200 °C and 300 °C. The reservoir at an initial geothermal source temperature of 200 °C degrades at an average rate of 1.9 °C per year and Sc CO_2 temperature decreases at the average rate of 2.7 °C per year correspondingly over a period of 25 years. For the geothermal reservoir containing high enthalpy heat with initial geothermal source temperature of 300 °C, the thermal degradation occurs at a faster rate of 4 °C per year. During the process of geothermal heat extraction, the temperature of Sc CO_2 absorbing the heat energy from a geothermal reservoir at an initial temperature of 300 °C decreases by 5.3 °C over a period of 25 years.

9.3. Production well

The temperature profile and pressure profile of Sc CO_2 flowing through the production well is shown in Figs. 4a and 5a, respectively, for a geothermal source temperature of 200 °C and in Figs. 4b and 5b, respectively, for a geothermal source temperature of 300 °C. The temperature of Sc CO_2 decreases continuously as it rises from the reservoir outlet through the casings to the outlet of the production well. Under adiabatic conditions assumed along the length of the casing, the flow is isenthalpic. The temperature changes in the isenthalpic flow are mainly due to the expansion of the fluid through the pipes of increasing diameter associated with Joule–Thompson effect as the fluid flows from the bottom to the top of the production well (Pruess, 2006). The temperature of Sc CO_2 at

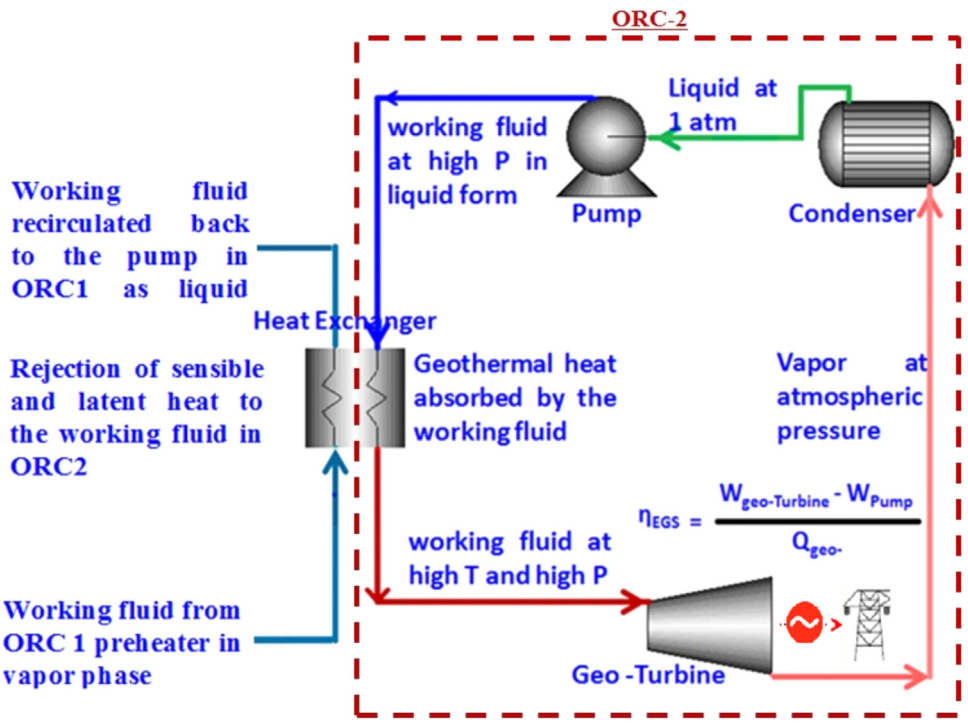

Fig. 7. Configuration of second ORC for the utilization of sensible and latent heat from the working fluid in ORC1 for power generation in EGS.

the outlet of the production well depends upon the temperature of Sc CO_2 at the reservoir outlet which in turn depends upon the life of the reservoir.

The temperature and pressure of Sc CO_2 at the outlet of the production well is tabulated in Tables 5a and 5b for the two geothermal source temperatures 200 °C and 300 °C, respectively. For a reservoir volume of 2.5 km^3 with 10 mD permeability and 50 m fracture spacing, the pressure of Sc CO_2 at the outlet of the production well is greater than the injection pressure for two different geothermal sources. The pressure of Sc CO_2 at the outlet of the production well depends strongly on the geothermal source temperature and the age of the reservoir. For certain reservoir geometry, higher geothermal source temperature gives rise to higher Sc CO_2 pressure at the outlet of the production well with a potential for expansion as a primary working fluid in the high pressure turbine for the generation of electricity. For a reservoir volume of 2.5 km^3 and a fracture spacing of 50 m, irrespective of the permeability, mining a geothermal source of 300 °C is more advantageous than a source at 200 °C.

Table 8a
Variation in the Net EGS power output for a geothermal reservoir 2.5 km^3, 10 mD and 50 m fracture spacing initially at 200 °C over 25 years with isobutane as working fluid in ORC1.

Cycle	Heat source	Conditions for the ORC cycle						Net EGS output (MW_e)
		Working fluid	Mass flow (kg/s)	P (MPa)	Preheat (%)	Power (MW_e)	η (%)	
ORC1	CO_2 at $t = 0$	Isobutane	350	0.5	2	18.9	10.1	46.9
ORC2	Isobutane-ORC1	Ammonia	107.5	0.25	0	10	5.9	
	CO_2 expansion in high pressure turbine					18		
ORC1	CO_2 at $t = 5$	Isobutane	325	0.6	0	18.7	10.9	42.3
ORC2	Isobutane-ORC1	Ammonia	100	0.25	0	8.6	6.6	
	CO_2 expansion in high pressure turbine					15		
ORC1	CO_2 at $t = 10$	Isobutane	325	0.6	10	18.3	12	34.5
ORC2	Isobutane-ORC1	Ammonia	90	0.2	0	5.2	3.9	
Case C	CO_2 expansion in high pressure turbine					11		
ORC1	CO_2 at $t = 15$	Isobutane	280	0.75	5	16.6	12.6	27.8
ORC2	Isobutane-ORC1	Ammonia	79	0.16	0	3.2	2.8	
Case C	CO_2 expansion in high pressure turbine					8		
ORC1	CO_2 at $t = 20$	Isobutane	250	0.6	7.5	13.4	9.8	21.3
ORC2	Isobutane-ORC1	Ammonia	68	0.16	0	2.9	2.5	
Case D	CO_2 expansion in high pressure turbine					5		
ORC1	CO_2 at $t = 25$	Isobutane	225	0.6	5	11.4	11.5	15.8
ORC-2	Isobutane-ORC1	Ammonia	61	0.13	0	1.4	1.6	
Case D	CO_2 expansion in high pressure turbine					3		

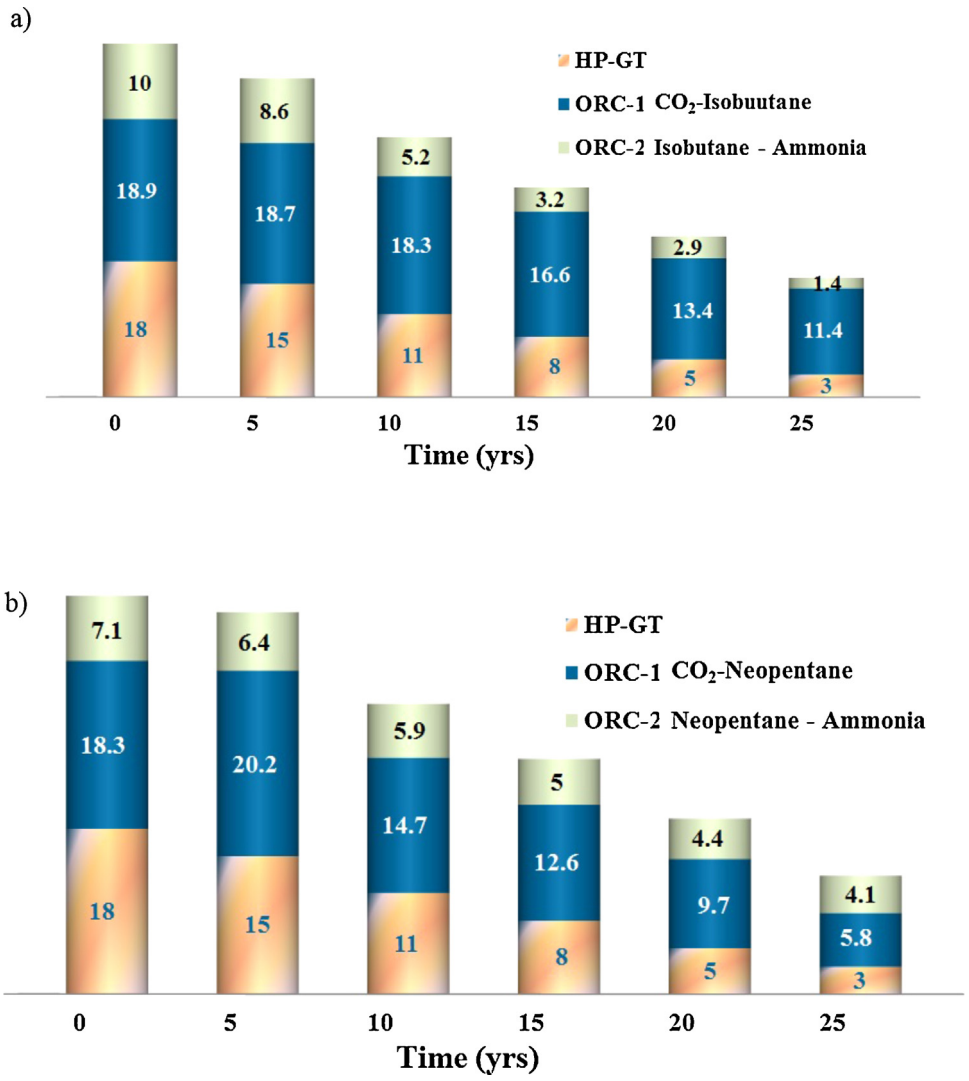

Fig. 8. Net EGS power output (MW_e) from a geothermal reservoir 2.5 km^3, 10 mD and 50 m fracture spacing at an initial temperature of 200 °C and ammonia in the second Rankine cycle for a period of 25 years.

As the pressure of Sc CO_2 at the outlet of the production well is greater than the injection pressure, expansion of the high pressure Sc CO_2 in a turboexpander to the injection pressure is necessary for subsequent recirculation to form a closed loop of heat transfer fluid circulation.

Based on the variation of the temperature of Sc CO_2 as a function of time from the reservoir at two geothermal source temperatures 200 °C and 300 °C, the magnitude of power generated in the turboexpander due to the expansion of the primary working fluid, Sc CO_2, is tabulated in Tables 5a and 5b, respectively. From Table 5a for a geothermal source at 200 °C, it can be seen that the power output from the high pressure turbine decreases continuously from 18 MW_e initially to 3 MW_e over a period of 25 years. From Table 5b for a geothermal source temperature of 300 °C, the power generated decreases from 44 MW_e initially to 9 MW_e over a period of 25 years. The time-averaged power output from the high pressure turboexpander is 6 MW_e for a geothermal source temperature of 200 °C and 17.9 MW_e for a geothermal source temperature of 300 °C over a period of 25 years. In all the cases, the Sc CO_2 is discharged from the high pressure turbine at 15 MPa so that it can recirculated back into the geothermal well. In all the cases, substantial amount of thermal energy is retained in Sc CO_2 after expansion in the high pressure turboexpander. Therefore, this geothermal energy can be utilized in an organic Rankine cycle for additional power generation in EGS. Based on the variation of the temperature of primary working fluid, Sc CO_2, as a function of time at the outlet of the turboexpander, the power output from the ORC is calculated for five different secondary working fluids isobutane, ammonia, *n*-butane, neopentane and isopentane. These values are tabulated in Tables 6a and 6b for the two geothermal source temperatures 200 °C and 300 °C, respectively.

9.4. Organic Rankine cycle

For the geothermal source temperature of 200 °C and 300 °C, the variation of power output generated in ORC is shown in Fig. 6a and b, respectively, for four different secondary working fluids for a period of 25 years. The parameters that are necessary to generate the power output from ORC for each working fluid is given in Table 6a for an initial geothermal source of 200 °C and Table 6b for an initial geothermal source temperature of 300 °C. The secondary working fluids, isobutane, ammonia and *n*-Butane effectively utilize the low-enthalpy geothermal heat energy and generate higher amount of electricity while isopentane and neopentane generate lower amount of electricity. The power output for each working fluid and the efficiency decrease steadily over a period of 25 years due to ageing of the geothermal reservoir associated with thermal degradation. The time-averaged net EGS power output over a

Table 8b
Variation in the Net EGS power output for a geothermal reservoir 2.5 km^3, 10 mD and 50 m fracture spacing initially at 200 °C over 25 years with neopentane as working fluid in ORC1.

Cycle	Heat source	Conditions for the ORC cycle						Net EGS output (MW_e)
		Working fluid	Mass flow (kg/s)	P (MPa)	Preheat (%)	Power (MW_e)	η (%)	
ORC1	CO_2 at t = 0	Neopentane	425	0.5	3.5	18.3	9.7	43.4
ORC2	Neopentane-ORC1	Ammonia	115	0.2	0	7.1	4.2	
	CO_2 expansion in high pressure turbine					18		
ORC1	CO_2 at t = 5	Neopentane	400	0.8	0	20.2	11.8	41.6
ORC2	Neopentane-ORC1	Ammonia	102	0.2	0	6.4	4.2	
	CO_2 expansion in high pressure turbine					15		
ORC1	CO_2 at t = 10	Neopentane	375	0.5	0	14.7	9.6	31.6
ORC2	Neopentane-ORC1	Ammonia	92	0.2	0	5.9	4.3	
Case C	CO_2 expansion in high pressure turbine					11		
ORC1	CO_2 at t = 15	Neopentane	325	0.5	0	12.6	9.6	25.6
ORC2	Neopentane-ORC1	Ammonia	80	0.2	0	4.96	4.2	
Case C	CO_2 expansion in high pressure turbine					8		
ORC1	CO_2 at t = 20	Neopentane	275	0.4	0	9.7	8.4	19.1
ORC2	Neopentane-ORC1	Ammonia	70	0.2	0	4.4	4.2	
Case D	CO_2 expansion in high pressure turbine					5		
ORC1	CO_2 at t = 25	Neopentane	250	0.25	0	5.8	5.8	12.9
ORC-2	Neopentane-ORC1	Ammonia	62.5	0.2	0	4.1	4.3	
Case D	CO_2 expansion in high pressure turbine					3		

period of 25 years is given in Table 7. For a reservoir at an initial geothermal source temperature of 200 °C, isobutane gives a maximum power output of 21 MW_e and isopentane gives a minimum power output of 14 MW_e. For a reservoir at an initial geothermal source temperature of 300 °C, a maximum power output of 46 MW_e was obtained from isobutane and a minimum power output of 36 MW_e was obtained from isopentane. When high-enthalpy geothermal heat energy (300 °C) is extracted, presence of the preheater initially facilitates the transfer of sensible heat from the superheated vapor leaving the turbine at atmospheric pressure to the cold incoming liquid at high pressures. Due to the thermal degradation of the geothermal reservoir, presence of preheater does not have any advantage in maximizing the utilization of geothermal heat energy after approximately 15 years. When low-enthalpy geothermal heat energy (200 °C) is utilized for electricity generation, presence of a preheater does not add any significant advantage as the amount of heat energy extracted in the preheater is not significant.

In the organic Rankine cycle, after the expansion of the working fluid in the ORC turbine, it is in a superheated state at atmospheric pressure. Even though, recuperator transfers some amount of sensible heat energy to the cold high pressure liquid, the latent heat of the working fluid is rejected in the condenser. To utilize the latent heat rejected in the condenser, a second organic Rankine cycle (ORC2) shown in Fig. 7 is cascaded with ammonia as a tertiary working fluid for all the cases. The secondary working fluid leaving the turbine in the superheated state in the first ORC (ORC1) transfers all the heat energy to ammonia in the heat exchanger, changes to liquid phase completely and is returned back to the pump in the first organic Rankine cycle. Ammonia absorbs the sensible and latent heat from the secondary working fluid used in the first organic Rankine cycle, goes completely to vapor phase and upon expansion in the high pressure turbine produces electricity. With isobutane and neopentane as secondary working fluids in the first organic Rankine cycle (ORC1) and ammonia as a tertiary working fluid in ORC2, the maximum amount of electricity that can be generated from the geothermal reservoir at an initial temperature of 200 °C is shown in Fig. 8a and b, respectively. The parameters used for maximizing the power output for both the cases are tabulated in Tables 8a and 8b. The time-averaged net EGS power output shown in Table 9 suggests that an additional 3 MW_e can be obtained with ORC2 when isobutane is used as a secondary working fluid in ORC1 and an additional 4.5 MW_e can be obtained from ORC2 with neopentane as a secondary working fluid in ORC1 over a period of 25 years. Even though, the efficiency in ORC2 is lower than that in ORC1, the low-enthalpy latent heat of the working fluid in ORC1 can be utilized for the additional amount of electricity generation.

The efficiency lost in an oxygen-fired IGCC plant with 75% carbon capture and sequestration varies between 6% and 10% (Rubin et al., 2012; Buhre et al., 2005). Assuming an average efficiency loss of 8% in carbon capture and sequestration based on this literature, the amount of energy lost in CCS is 50MW_e for a 629 MW_e IGCC plant. From Table 7, it can be seen that over a period of 25 years, by choosing the right kind of working fluid, with a reservoir initially at 300 °C, significant amount of the energy lost can be recovered (92% with isobutane and 74% with neopentane). From Table 9, it can be seen that, for an initial reservoir temperature of 200 °C, the energy recovery is 48% with isobutane as a working fluid and 43% with neopentane as a working fluid. Among the fluids modeled for ORC in this study, isobutane gives the maximum power output at all geothermal source temperatures. Even though neopentane and isopentane produce lower power output among the fluids modeled in this study, these two fluids are more suitable for arid regions due to their higher boiling points that eliminate the necessity to use a chiller. Cascading a second organic Rankine cycle to utilize the sensible and latent heat of the secondary working fluid from the first organic Rankine cycle can be considered for a the geothermal

Table 9
Time-averaged net power output (MW_e) from EGS over a period of 25 years from a reservoir of volume 2.5 km^3, 10 mD and 50 m fracture spacing with an initial geothermal source temperature of 200 °C.

	Isobutane (MW_e)	Neopentane (MW_e)
HPGT* + ORC1	21	17
HPGT* + ORC1 + ORC2	24	21.5

* HPGT—high pressure gas turbine output.

source at 200 °C to produce an additional power output of 4.5 MW_e with neopentane as secondary working fluids over a period of 25 years.

10. Conclusion

Among the technologies that are available for power generation, pairing a coal-fired IGCC plant with EGS facilitates the simultaneous extraction of geothermal heat energy and sequestration of CO_2. The pressure of Sc CO_2 leaving the production well is greater than the injection pressure, in addition to the geothermal heat energy. Therefore, adding a high pressure turboexpander before an organic Rankine cycle maximizes the conversion of geothermal heat to electricity while reducing the pressure of Sc CO_2 to the injection pressure for subsequent recirculation in a steady state process. Pairing IGCC with a geothermal reservoir initially at 300 °C in a semi-arid region facilitates the recovery of 74% of the energy lost in the carbon capture and sequestration process with neopentane as secondary working fluid by producing a time-averaged EGS power output of 37 MW_e over a period of 25 years.

$$\alpha = \frac{(W)^3}{(12 \times S)} \tag{1}$$

$$\varepsilon = \left(\alpha^{1/3}\right)\left(S^{-2/3}\right)\left(12^{1/3}\right) \tag{2}$$

$$V_V = \varepsilon \times V \tag{3}$$

$$W_R = (V)^{1/3} \tag{4}$$

$$N_R = \frac{W_R}{S} \tag{5}$$

$$L = L_R \tag{6}$$

$$V_F = \frac{V_V}{N_F} \tag{7}$$

$$H = \frac{V_F}{(L \times W)} \tag{8}$$

$$A_C = W \times H \tag{9}$$

$$P = 2 \times (W + H) \tag{10}$$

$$D_H = 4 \times \frac{A_C}{P} \tag{11}$$

$$Re_D = \frac{\left(m_f \times D_H\right)}{(A_C \times \mu)} \tag{12}$$

$$Pr = \frac{C_p \mu}{k} \tag{13}$$

$$\beta = -\left(\frac{1}{\rho}\right)\left(\frac{\mathrm{d}\rho}{\mathrm{d}T}\right) \tag{14}$$

When the fracture spacing is 10 m,

$$Ra' = \frac{\rho^2 g \beta C_p W^4 (T_W - T_b)}{\mu k L} \tag{15}$$

$$Nu = \frac{Ra'}{24} \tag{16}$$

When Fracture spacing is 50 m, the Nusselt number is calculated by

Collier relation for channels with $L/D_H > 50$ and $Re < 2000$

$$Nu = 0.17 Re_D^{0.33} Pr_f^{0.43} \left[\frac{Pr_f}{Pr_w}\right]^{0.25} \left[\frac{g \beta D_H^3 (T_w - Tb)}{v_f^2}\right]^{0.1} \tag{17}$$

$$h = \frac{(Nu \times k)}{D_H} \tag{18}$$

$$A_H = 2 \times L \times (W + H) \tag{19}$$

The overall heat transfer coefficient is given by

$$UA_H = \left(\frac{1}{hA_H} + \frac{x}{kA_H}\right)^{-1} \tag{20}$$

$$Bi = \frac{UD_H}{k_S} \tag{21}$$

Using lumped parameter analysis, the rock temperature is given by

$$\frac{T_{R,t} - T_{F,0}}{T_{R,0} - T_{F,0}} = \mathrm{Exp}\left(\frac{UA_H t}{\left(\rho_R (\mathrm{LHS}) C_{\mathrm{PR}}\right)}\right) \tag{22}$$

$$Q_{R,t} = \rho_R \times (\mathrm{LHS}) \times C_{\mathrm{PR}} \times \left(T_{R,t} - T_{\mathrm{Ambient}}\right) \tag{23}$$

$$Q_{R,t+1} = \rho_R \times (LHS) \times C_{PR} \times \left(T_{R,t+1} - T_{\mathrm{Ambient}}\right) \tag{24}$$

$$\Delta Q = Q_{R,t+1} - Q_{R,t} \tag{25}$$

$$\Delta Q = m_f \times C_P \times \left(T_{F,t} - T_{F,0}\right) \times (\Delta t) \tag{26}$$

Acknowledgments

This material is based upon work supported by the United States Department of Energy under Award Number DE-EE0002739 and American Recovery and Reinvestment Act (ARRA) funds.

References

Adams, B.M., Kuehn, T.H., Bielicki, J.M., Randolph, J.B., Saar, M.O., 2014. On the importance of the thermosiphon effect in CPG (CO_2 plume geothermal) power systems. Energy 69 (0), 409–418.
Aljundi, I.H., 2011. Effect of dry hydrocarbons and critical point temperature on the efficiencies of organic Rankine cycle. Renewable Energy 36 (4), 1196–1202.
Atrens, A.D., Gurgenci, H., Rudolph, V., 2009. CO_2 thermosiphon for competitive geothermal power generation. Energy Fuels 23 (1), 553–557.
Atrens, A.D., Gurgenci, H., Rudolph, V., 2010. Electricity generation using a carbon-dioxide thermosiphon. Geothermics 39 (2), 161–169.
Bachu, S., 2008. CO_2 storage in geological media: role, means, status and barriers to development. Prog. Energy Combust. Sci. 34 (2), 254–273.
Blackwell, D.D., Richards, M., 2004. Geothermal Map of North America. Amer. Assoc. Petroleum Geologists, I sheet, scale 1:6,500,000.
Brasz, Lars J., Bilbow, William M., 2004. Ranking of working fluids for organic Rankine cycle applications. In: International Refrigeration and Air Conditioning Conference, Purdue, pp. 722–729.
Brown, D.W., 2000. A hot dry rock geothermal energy concept utilizing supercritical CO_2 instead of water. In: Proceeding, Twenty-Fifth Workshop on Geothermal Reservoir Engineering, Jan 24–26, Stanford University, Stanford, California, Stanford University, Stanford, California.
Bruhn, M., 2002. Hybrid geothermal–fossil electricity generation from low enthalpy geothermal resources: geothermal feedwater preheating in conventional power plants. Energy 27 (4), 329–346.
Buhre, B.J.P., Elliott, L.K., Sheng, C.D., Gupta, R.P., Wall, T.F., 2005. Oxy-fuel combustion technology for coal-fired power generation. Prog. Energy Combust. Sci. 31 (4), 283–307.
Chen, H., Goswami, D.Y., Stefanakos, E.K., 2010. A review of thermodynamic cycles and working fluids for the conversion of low-grade heat. Renewable Sustainable Energy Rev. 14 (9), 3059–3067.
DiPippo, R., 1999. Small geothermal power plants: design, performance and economics. GHC Bull. 20 (2), 1–8.
Duchane, D.V., 1996. Geothermal energy from hot dry rock: a renew able energy technology moving towards practical implementation. Renewable Energy 9 (1–4), 1246–1249.
Edrisi, B.H., Michaelides, E.E., 2013. Effect of the working fluid on the optimum work of binary-flashing geothermal power plants. Energy 50 (0), 389–394.
Figueroa, J.D., Fout, T., Plasynski, S., McIlvried, H., Srivastava, R.D., 2008. Advances in CO_2 capture technology—The U.S. Department of Energy's Carbon Sequestration Program. Int. J. Greenhouse Gas Control 2 (1), 9–20.
Frank, E.D., Sullivan, J.V., Wang, M.Q., 2012. Life cycle analysis of geothermal power generation with supercritical carbon dioxide. Environ. Res. Lett. 7 (3), 034030.
Guo, T., Wang, H.X., Zhang, S.J., 2011. Fluids and parameters optimization for a novel cogeneration system driven by low-temperature geothermal sources. Energy 36 (5), 2639–2649.
Heberle, F., Preißinger, M., Brüggemann, D., 2012. Zeotropic mixtures as working fluids in organic Rankine cycles for low-enthalpy geothermal resources. Renewable Energy 37 (1), 364–370.
Kramer, D., 2012. Scientists poke holes in carbon dioxide sequestration. Phys. Today 65 (8), 22–24.

Lai, N.A., Wendland, M., Fischer, J., 2011. Working fluids for high-temperature organic Rankine cycles. Energy 36 (1), 199–211.
Liu, B.-T., Chien, K.-H., Wang, C.-C., 2004. Effect of working fluids on organic Rankine cycle for waste heat recovery. Energy 29 (8), 1207–1217.
Madhawa Hettiarachchi, H.D., Golubovic, M., Worek, W.M., Ikegami, Y., 2007. Optimum design criteria for an organic Rankine cycle using low-temperature geothermal heat sources. Energy 32 (9), 1698–1706.
Mock, J.E., Tester, J.W., Wright, P.M., 1997. Geothermal energy from the earth: its potential impact as an environmentally sustainable resource. Annu. Rev. Energy Environ. 22, 305–356.
Polsky, Yarom, Capuano, LouisJJr., Finger, John, Huh, Michael, Knudsen, Steve, Chip Mansure, A.J., Raymond, David, Swanson, Robert, December 2008. Enhanced Geothermal Systems (EGS) Well Construction Technology Evaluation Report. Sandia National Laboratories (p 108 Pages).
Nelson, C.R., Evans, J.M., Sorensen, J.A., Steadman, E.N., Harju, J.A., Evans, J.M., Sorensen, J.A., Steadman, E.N., Harju, J.A., 2005. Factors Affecting the Potential for CO_2 Leakage from Geological Sinks, ⟨http://www.undeerc.org/PCOR/newsandpubs/pdf/FactorsAffectingPotential.pdf⟩.
Pritchett, J.W., 2009. In on the relative effectiveness of H_2O and CO_2 as reservoir working fluid for EGS heat mining. Geotherm. Res. Counc. Trans. 33, 235–239.
Pruess, K., 2006. Enhanced geothermal systems (EGS) using CO_2 as working fluid—a novel approach for generating renewable energy with simultaneous sequestration of carbon. Geothermics 35 (4), 351–367.
Pruess, K., 2008. On production behavior of enhanced geothermal systems with CO_2 as working fluid. Energy Convers. Manage. 49 (6), 1446–1454.
Quoilin, S., Broek, M.V.D., Declaye, S., Dewallef, P., Lemort, V., 2013. Techno-economic survey of organic Rankine cycle (ORC) systems. Renewable Sustainable Energy Rev. 22 (0), 168–186.
Randolph, J.B., Saar, M.O., 2011a. Combining geothermal energy capture with geologic carbon dioxide sequestration. Geophys. Res. Lett. 38 (10), 1–7, Paper #L10401.
Randolph, J.B., Saar, M.O., 2011b. Coupling carbon dioxide sequestration with geothermal energy capture in naturally permeable, porous geologic formations: Implications for CO_2 sequestration. Energy Procedia 4, 2206–2213.
Rubin, E.S., Mantripragada, H., Marks, A., Versteeg, P., Kitchin, J., 2012. The outlook for improved carbon capture technology. Prog. Energy Combust. Sci. 38 (5), 630–671.
Saleh, B., Koglbauer, G., Wendland, M., Fischer, J., 2007. Working fluids for low-temperature organic Rankine cycles. Energy 32 (7), 1210–1221.
Sanyal, S.K., Butler, S.J., 2005. An analysis of power generation prospects from enhanced geothermal systems. Geotherm. Resour. Counc., Trans. 29.
Schuster, A., Karellas, S., Aumann, R., 2010. Efficiency optimization potential in supercritical organic Rankine cycles. Energy 35 (2), 1033–1039.
Sotirios, K., Andreas, S., 2010. Supercritical fluid parameters in organic Rankine cycle applications. Int. J. Thermodyn. 11 (3), 101–108.
The Future of Geotherrmal Energy, 2006. Impact of Enhanced Geothermal Systems (EGS) on the United States in the 21st Century. Massachusetts Institute of Technology, pp. 372.
U.S Carbon dioxide emissions from energy consumption. Annual Energy Review August 2012. ⟨http://www.eia.gov/environment/data.cfm#summary⟩ (accessed on March 24, 2014).
U.S. Energy Information Administration, 2012. Annual Energy Review 2011. U.S. Energy Information Administration, ⟨http://www.eia.gov/totalenergy/data/annual/showtext.cfm?t=ptb0802c⟩ (DOE/EIA-0384(2011)).
White, C.M., Straziser, B.R., Granite, E.J., Hoffman, J.S., Pennline, H.W., 2003. Separation and capture of CO_2 from large stationary resources and sequestration in geological formulations—coalbeds and deep saline aquifers. J. Air Waste Manage. Assoc. 53, 645–715.